Constraints on climate change stabilization based on observations of Earth's energy imbalance

Geophysical Research Letters

RESEARCH LETTER
10.1029/2025GL121056

Constraints on Climate Change Stabilization Based on Observations of Earth's Energy Imbalance

Hervé Douville[1] **and Richard P. Allan**[2]

[1]Météo-France, CNRS, University Toulouse, CNRM, Toulouse, France, [2]Department of Meteorology and National Centre for Earth Observation, University of Reading, Reading, UK

Key Points:

- Beyond the maximum level of global warming, the timing of the Earth's heating rate reversal is another key metric of climate change
- Observational constraints on CMIP6 projections make a reversal of EEI trends very unlikely before 2043 under the SSP1-2.6 scenario
- More research is needed to better understand why the Earth's heat imbalance is increasing faster than expected

Supporting Information:

Supporting Information may be found in the online version of this article.

Correspondence to:

H. Douville,
herve.douville@meteo.fr

Citation:

Douville, H., & Allan, R. P. (2026). Constraints on climate change stabilization based on observations of Earth's energy imbalance. *Geophysical Research Letters*, *53*, e2025GL121056. https://doi.org/10.1029/2025GL121056

Received 5 DEC 2025
Accepted 15 MAY 2026

Abstract The Earth's energy imbalance (EEI) at the top of the atmosphere is a key indicator of climate change that determines the Earth's heating rate. Here, we use a global reconstruction of surface temperature and EEI measurements to constrain global projections of the Earth heating rate until the end of the century. Our robust statistical method is shown to withstand changes in the prior distribution or the length of the EEI record, and to perform well when evaluated against independent pseudo-observations. Results show that the reversal of the Earth heating rate is very unlikely to occur before the early 2040s, even under a low emission scenario. This is more than 10 years later than expected from the raw projections, with significant implications for both mitigation and adaptation policies. Future research is however needed to better attribute the observed EEI changes and to explore the patterns of recent versus future EEI changes.

Plain Language Summary The Earth is currently gaining more energy from the Sun than it is losing back to space. This imbalance-called the Earth's Energy Imbalance (EEI) In this study, we combine global surface temperature data with measurements of this heat imbalance at the top of the atmosphere to estimate how fast the planet will keep warming through the rest of the century. For this purpose, we use a robust statistical method and test it in different ways to make sure the results are reliable. Our findings suggest that the Earth will keep gaining heat for at least the next couple of decades. Even in a scenario where greenhouse gas emissions are kept low, it's very unlikely that this warming trend will start to reverse before the early 2040s. This is more than 10 years later than earlier estimates suggested, which matters for planning how to reduce emissions and adapt to climate impacts. The study also notes that more research is needed to better understand why the Earth's heat imbalance is increasing faster than expected.

1. Introduction

Global warming is caused by a human-caused Earth energy imbalance (EEI) between the absorbed shortwave radiation (ASR) and the outgoing longwave radiation (OLR) at the top of the atmosphere (TOA). Positive EEI values derived from satellite instruments imply an energy accumulation within the climate system, at a rate which has more than doubled in recent decades (Forster et al., 2025; Mauritsen et al., 2025). This increase is much faster than simulated by global climate models and than expected from the sixth IPCC Assessment Report (AR6, Forster et al., 2021). Such a discrepancy between climate models and observations is still a matter of debate (Li et al., 2024; Mauritsen et al., 2025; Minière et al., 2025; Raghuraman et al., 2021, 2023; Samset et al., 2025) but underlines the need to ensure our ability to monitor and better anticipate the EEI variations in the long term (Mauritsen et al., 2025).

EEI has been included as a new indicator of climate change in the latest issue of the WMO report on the state of the global climate (WMO, 2026), with year 2025 showing the highest record since satellite observations began in the 1960's. This growing imbalance indicates that the total amount of heat stored on Earth is not just increasing but accelerating, as also supported by the increasing ocean heat content (Storto & Yang, 2024). Implications for climate projections are not clear given multiple source of uncertainties in both aerosol forcings and climate responses. Yet, if the current EEI is really larger than simulated, it means that the global ocean is absorbing more heat than expected, that more future warming is already locked in, and that the remaining carbon budget compatible with the Paris Agreement is smaller than anticipated.

The EEI metric is the bridge between energy accumulation and the carbon budget. Improving EEI projections is thus crucial to better anticipate our ability to stabilize climate change. A particular challenge is to predict how long it will take first to reverse EEI trends from positive to negative values, then to bring EEI back to zero physically

meaning that the Earth system will no longer accumulate heat, although the global mean surface temperature may still evolve due to heat redistribution within the Earth system. The main objective of the present study is to constrain these two metrics based on available projections from the sixth phase of the Coupled Model Intercomparison Project (CMIP6, Eyring et al., 2016) under two contrasted greenhouse gas (GHG) emission scenarios.

For this purpose, we will also use satellite radiative measurements from the Clouds and the Earth's Radiant Energy System (CERES, Smith et al., 2011) project (cf. Materials and Methods). The Energy Balanced and Filled (CERES-EBAF) data set provides TOA irradiances since March 2000, which are considered stable enough to study the EEI variability on multi-decadal timescales (e.g., Loeb, 2024; Loeb et al., 2018; von Schuckmann et al., 2023). Recently, the CERES-EBAF satellite record was extended back to 1985 (Liu & Allan, 2018; Liu et al., 2020) and was used to derive an increase in the global ocean surface warming by 0.54 ± 0.07°K for each GJ/m^2 of accumulated energy (Merchant et al., 2025). This EEI reconstruction was also combined with the ERA5 reanalysis (Hersbach et al., 2020) to better understand the positive EEI doubling between 2001–2014 and 2015–2023 (Allan & Merchant, 2025). In line with previous findings (Goessling et al., 2024), this doubling was found to arise primarily from an increase in absorbed sunlight related to cloud-radiative effects, but may not be representative of the long-term cloud response.

In the present study, the DEEP-C product (Liu & Allan, 2018) is used to constrain the forced EEI response derived from CMIP6 global climate projections, either in isolation or in combination with GSAT observations (Morice et al., 2020). Data and methods are not new and are thus briefly described in the enclosed Supporting Information S1. Monthly mean EEI and GSAT timeseries are first decomposed according to three typical timescales in order to highlight their complex intermodel relationships. The KCC Bayesian statistical method (Qasmi & Ribes, 2022) is then used to narrow modeling uncertainties in the EEI projections. The ultimate objective is to better anticipate the timing at which the accumulation of heat in the climate system is expected first to stabilize, then to stop. The main limitations of the study, but also the possibility of further improving the method, are discussed in the final section.

2. Results

2.1. GSAT Versus EEI Global Mean Timeseries

Looking at observations from January 1985 to December 2023, both GSAT and EEI monthly mean timeseries can be split into three additive components: a multi-decadal *trend*, a climatological annual cycle (hereafter *seasonality amplitude*), and a residual noise (hereafter *variability*). This is first illustrated for GSAT (Figures S1a–S1d in Supporting Information S1), where a linear fit of the trend component indicates an average rate of global warming of 0.23 ± 0.06°K per decade. The same decomposition can be applied to the EEI reconstruction (Figures S1e–S1h in Supporting Information S1), also featuring a strong annual cycle with an average amplitude much greater than the climate change signal. Deseasonalized EEI anomalies however show a significant positive linear trend of 0.43 ± 0.26 W/m^2 per decade, in line with previous studies (e.g., Merchant et al., 2025). This trend is very unlikely due to internal climate variability and was shown to arise from a combination of factors including a longwave cloud masking effect, but also shortwave cloud adjustments to increasing concentrations of GHG and to declining aerosols (Goessling et al., 2024; Hodnebrog et al., 2024; Raghuraman et al., 2023).

Figure 1 displays scatterplots of GSAT versus EEI statistics over the 1985–2023 period across our subset of CMIP6 models. First shown is the lack of relationship between the present-day climatologies (Figure 1a), as expected from the tuning of coupled models which mainly consists of reaching a zero EEI in preindustrial climate despite susbtantial systematics errors, including in GSAT. This interpretation is supported by a significant negative correlation ($R = -0.44$) between the present-day EEI climatology and the rate of global warming simulated over the 1985–2023 period across CMIP6 models (not shown), with models featuring the largest positive EEIs generally showing a lower than observed warming rate. Conversely, models that are close to the DEEP-C climatology tend to produce a stronger warming rate than the ERA5 reanalysis (Hersbach et al., 2020). This negative relationship suggests an equifinality problem whereby different combinations of radiative forcings and feedbacks lead to similar values of GSAT.

Figure 1b indicates a statistically significant positive correlation ($R = 0.45$) between the seasonality amplitude of EEI and GSAT respectively. This metric may thus be useful to better understand processes that control the GSAT response to a human-caused EEI increase at longer timescale. Assuming a normal distribution for both EEI and

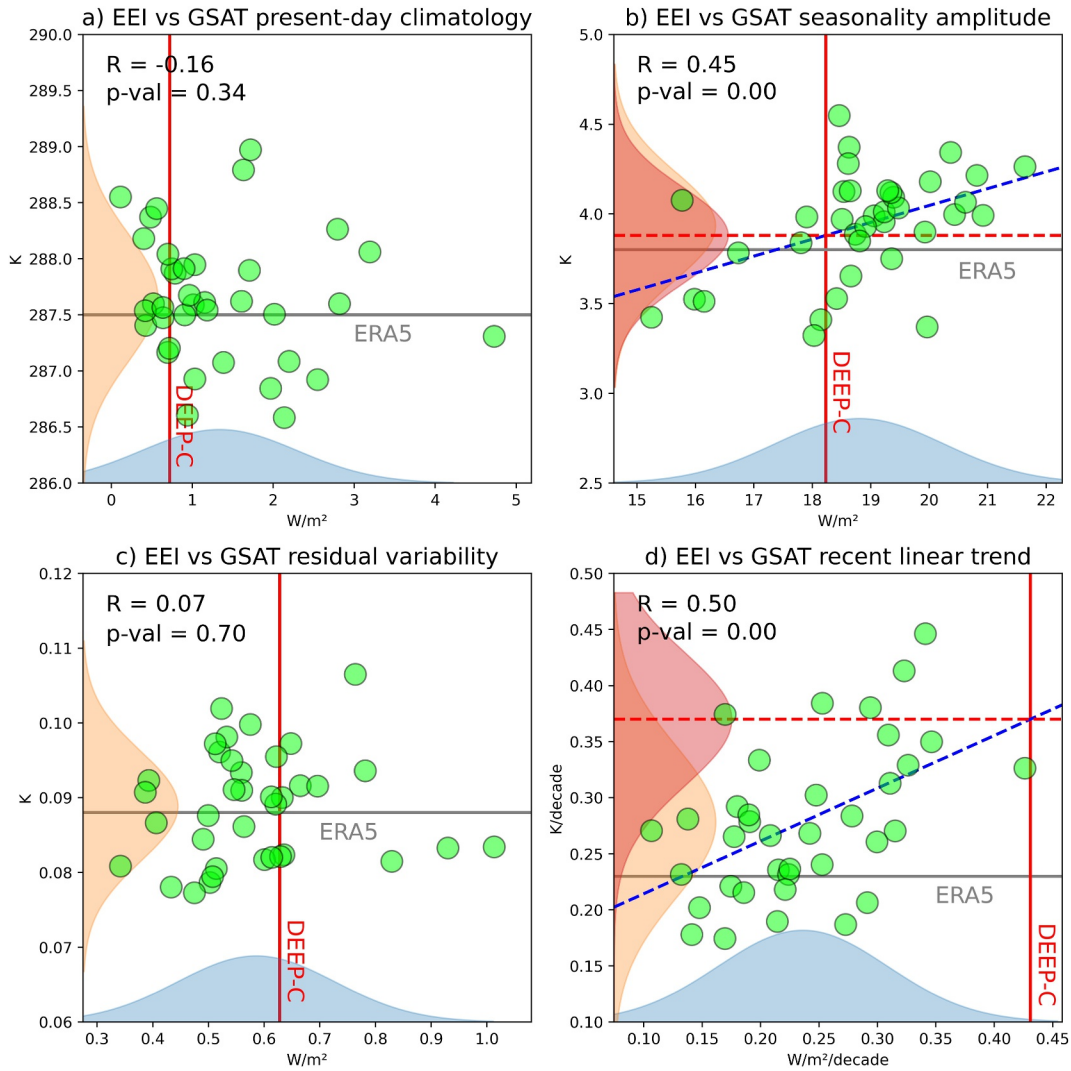

Figure 1. Scatterplots of EEI (W/m^2) versus GSAT (K) timescale components across CMIP6 models. (a) EEI vs. GSAT present-day climatology; (b) EEI vs. GSAT seasonality amplitude; (c) EEI versus GSAT residual variability (i.e., standard deviation of the residual noise shown in Figures S1d and S1h of Supporting Information S1 respectively); (d) EEI versus GSAT recent linear trend (unit per decade). Each green symbol represents a CMIP6 model and R denotes the correlation between the EEI and GSAT component, respectively. Normal model distributions are fitted on both axes. The red vertical (gray horizontal) line denotes the corresponding EEI (GSAT) metric derived from the DEEP-C (ERA5) data set. When the p-value of the correlation is less than 0.05, a multi-model linear fit is shown as a blue dashed line, a red horizontal dashed line is plotted to highlight the DEEP-C projection on the *y*-axis, and the *posterior* distribution of the GSAT component (i.e., conditional to the DEEP-C observations) is shown in red shading.

GSAT statistics, it is then possible to use Bayesian statistics to infer a posterior distribution of the GSAT seasonality amplitude based on the assumed linear relationship (e.g., Li, Liu, et al., 2025, Li, Zwiers, et al., 2025). The comparison of the prior and posterior distributions then suggests that some CMIP6 models overestimate the seasonality amplitude of both EEI and GSAT. This finding is broadly consistent with the GSAT seasonality amplitude found in ERA5 which is indeed lower than the CMIP6 ensemble mean value.

Although no link is found between EEI and GSAT regarding the magnitude of their residual variability (Figure 1c), the trend components show a significant 0.5 correlation (Figure 1d). This result suggests that the observed EEI trends can be useful to assess climate sensitivity (e.g., Olonscheck & Rugenstein, 2024). A straightforward application of Bayesian statistics however leads to a paradox. While most CMIP6 models underestimate the observed EEI trend, they tend conversely to overestimate the observed global warming. This paradox may arise from several non-exclusive explanations, which will be discussed later on in Section 3.

Similar scatterplots can be used to focus on the shortwave and longwave EEI contributions separately. Looking first at ASR (Figure S2 in Supporting Information S1), the inter-model relationship with GSAT trends is much stronger ($R = 0.81$) than for EEI but there is no significant relationship with GSAT seasonality. This suggests a key role for anthropogenic aerosols in the intermodel spread of both ASR and GSAT trends, in line with the conclusion of Skeie et al. (2024). As expected, the OLR shows a significant relationship with GSAT seasonality, with greater GSAT associated with larger longwave cooling (Figure S3 in Supporting Information S1). Yet, the strongest relationship with GSAT is again found for the trend component ($R = 0.84$).

These scatterplots suggests a combined influence of both GHG and aerosols on recent GSAT variations. Yet, future changes in GSAT may be mostly influenced by GHG emissions since the anthropogenic aerosol forcing is expected to decrease in all emission scenarios. Moreover, our specific objective here is not to constrain GSAT projections, but rather to better anticipate the stabilization of climate change on the basis of EEI projections. Before using KCC, let's first illustrate the relationship between recent and future EEI changes across CMIP6 models.

2.2. Constraining CMIP6 Projections of EEI With Observations

Early attempts to constrain CMIP6 projections have mainly focused on GSAT. In particular, Tokarska et al. (2020) have used an emergent intermodel relationship between the recent and future rates of global warming to condition GSAT projections on the observed warming rate. This simple technique, first proposed by Douville and Plazzotta (2017), is illustrated in Figure S5 of Supporting Information S1. Three global spatial domains are here considered: all grid cells, ocean only and land only. The scatterplots support the emerging constraint used by Tokarska et al. (2020), with 53% of the intermodel spread in future GSAT changes accounted for by the inter-model spread in the recent warming rate. Figure S6 in Supporting Information S1 shows similar scatterplots for EEI trends versus future EEI changes. The emergent relationship is even stronger than for GSAT, hence suggesting that the method could be also suitable for constraining EEI projections. The recent warming rate shows a weaker link with future EEI changes (Figure S7 in Supporting Information S1), thus highlighting the difficulty to constrain EEI projections only with GSAT observations.

The objective of the present study is to take advantage of the KCC method developed at CNRM (Qasmi & Ribes, 2022), which allows us to condition EEI projections not only on EEI or GSAT records, but also on their combination. This Bayesian method has proven successful in many former applications (e.g., Douville, 2023; Douville et al., 2022; Douville & Willett, 2023; Li, Liu, et al., 2025, Li, Zwiers, et al., 2025) and is here applied to a large subset of CMIP6 models under two contrasted emission scenarios (Figure 2). Starting with the SSP5-8.5 high emission scenario, the EEI response is first constrained with the HadCRUT5 ensemble GSAT reconstruction (Figure 2a). In spite of the results shown in Figure S7 of Supporting Information S1, a significant narrowing of the 5%–95% confidence interval (CI) is obtained, by 18% in the middle of the 21st century, associated with a negative shift of the best estimate. In contrast, constraining the simulated EEI evolution with the DEEP-C reconstruction shifts the distribution upward and leads to a marginal CI reduction (Figure 2b). This apparent paradox will be discussed in Section 3. In pratice, the merging of both observational constraints allows KCC to further narrow the CMIP6 modeling uncertainty by 35% in 2050 (Figure 2c). The ensemble mean forced EEI response is shifted upward, thus implying a delayed climate change stabilization.

Similar qualitative conclusions can be drawn from the SSP1-2.6 low-emission scenario (Figures 2d–2f). The results again show a synergy between the two observational constraints (as emphasized by the CIR metric) with a 2050 reduction of the 5%–95% confidence interval again close to 30% when combining them. The signal-to-noise ratio is here much weaker than under the SSP5-8.5 scenario, yet the results are consistent and further support the possibility of using a single realization of each model to derive the prior distribution of the forced EEI response. Note that KCC assumes a normal distribution so that it does not use the individual model realizations but only needs the ensemble mean forced response and its standard deviation. In other words, the method is more robust than most linear regression techniques which can be much more sensitive to spurious outliers influenced by internal climate variability.

The KCC constraint on the SSP1-2.6 projections has significant implications regarding the timing of climate stabilization (Figure 3). The ensemble mean [and 5%–95% confidence interval of the timing of trend reversal is 2050 (2032–2064) in the raw projections against 2053 (2043–2064) after being constrained with KCC. In other words, the EEI stabilization occurs at best 11 years later in the constrained projections, as indicated by the lower

10.1029/2025GL121056

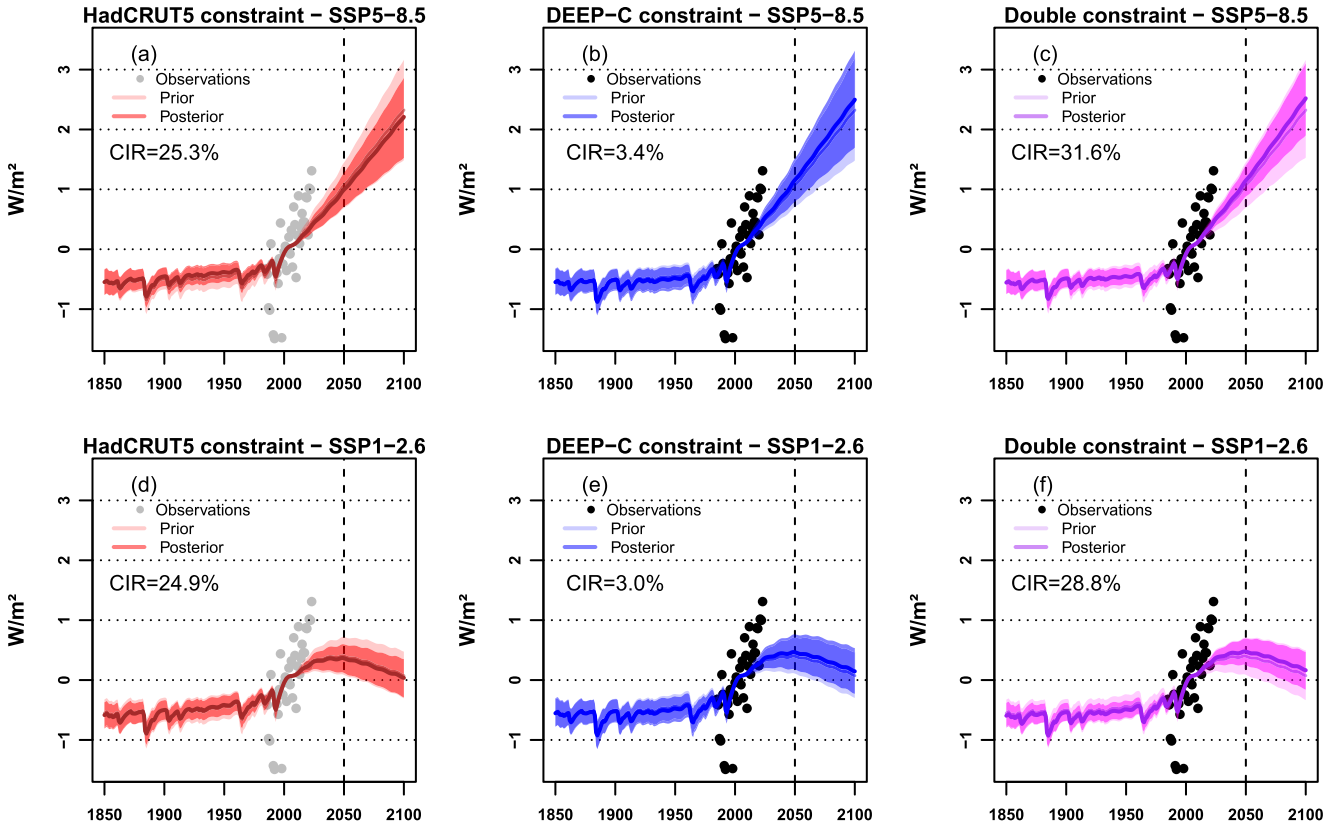

Figure 2. Constrained versus unconstrained annual mean forced changes in Earth's Energy Imbalance (W/m^2) for two contrasted emission scenarios. Mean (solid lines) and 5%–95% range (shading) of the prior and posterior distributions of the annual mean EEI response to both natural and anthropogenic radiative forcings in historical simulations and the SSP5-8.5 high-emission scenario: (a) HadCRUT5-only observational constraint; (b) DEEP-C-only observational constraint; (c) Combined HadCRUT5 and DEEP-C observational constraints on EEI. (d, e, f) Same as (a, b, c) but for the SSP1-2.6 low-emission scenario. The observed EEI anomalies are shown as black (gray) filled circles when they are (not) used for constraining the model response. The black vertical dashed line denotes the middle of the 21st century. All anomalies are relative to the 1995–2014 climatology. The CIR denotes the percentage reduction of the 5%–95% confidence interval in 2050 when comparing the constrained versus unconstrained distributions. Note that the 11-year oscillation due to prescribed natural variability of the solar forcing is apparent in all simulations (albeit hidden by the strong anthropogenic radiative forcing in the SSP5-8.5 scenario) and that the radiative effect of major volcanic eruptions in the 20th century are accounted in KCC for via a simple Energy Balance Model (cf. SI).

bound of the 5%–95% CI. Similarly, the ensemble mean timing of EEI cancellation occurs in 2549 (2238–3060) in the raw projections, against 2581 (2277–3032) after constraint. CIs are here very large given the crude linear extrapolation method which has been used to expand the projections after 2100. The SSP1-2.6-Ext projections expanded until 2300 could have been used, but would have led us to use a much weaker number of CMIP6 models. Arguably, the timing of EEI trend reversal is the most policy-relevant metric given the fundamental difficulty to anticipate future GHG emissions despite the Paris Agreement. The EEI cancellation timing however reminds us of the long-term implications of current policy decisions.

2.3. Method Evaluation

Besides KCC, many other statistical techniques have been proposed to constrain global climate projections, but most of them have been shown to be quite sensitive to the choice of the prior distribution and, for instance, did not withstand the transition from CMIP5 to CMIP6 (Ferguglia et al., 2023; Schlund et al., 2020). Many empirical emergent constraints are based on a linear regression framework and have the potential to produce overconfident projections (Sanderson et al., 2021). Although former applications of KCC have led to consistent results across several generations of CMIP models (e.g., Douville & Willett, 2023; Ribes et al., 2021), it is thus crucial to check that our posterior distribution is not much changed when replacing CMIP6 by CMIP5 projections (Figure S8 in Supporting Information S1).

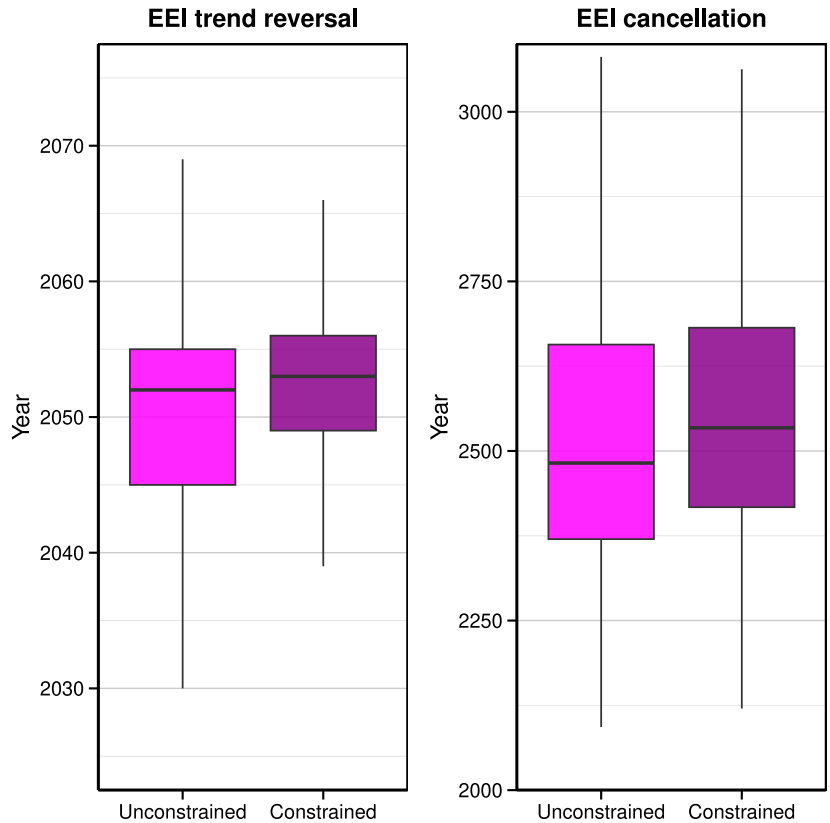

Figure 3. Box-and-whiskers plots of constrained versus unconstrained estimates of the timing of climate stabilization based on two definitions: EEI trend reversal (left panel) and EEI cancellation (right panel). The median of the distribution is highlighted by a thick line, the box corresponds to the interquartile range (IQR = Q3–Q1) and the whiskers denote the Q1 − 1.5*IQR and Q3 + 1.5*IQR values respectively. EEI trend reversal was estimated from linear trends calculated over 21-year rolling windows, while EEI cancellation was estimated by extrapolating linearly the last 30 years of the EEI forced responses and accounting for the non-zero 1995–2014 climatology.

Another evaluation strategy is the cross-validation method proposed by Ribes et al. (2021). One single historical simulation of one CMIP6 model is considered as pseudo-observations, thus enabling to test whether the KCC method is capable of predicting the forced response projected by this model. For this purpose, the other CMIP6 models are used to construct the prior and to calculate the posterior distribution constrained by these pseudo-observations. By repeating this leave-out-one procedure with each available CMIP6 model, it is then possible to assess the relevance of the corrections made by KCC to the future climate response by comparing the constrained versus unconstrained distributions to the pseudo-observations.

Here we use an even more stringent evaluation method where pseudo-observations are derived from CMIP5 models. In doing so, we account for potential discrepancies in the anthropogenic aerosol radiative forcing (e.g., Hodnebrog et al., 2024) and we overcome the interdependency between some CMIP6 models, which may only differ by their geochemistry or their horizontal resolution. The KCC performance is simply estimated as the root mean square error (RMSE) between the CMIP6 ensemble mean forced response and the CMIP5 pseudo-observations over the future 2026–2100 period. Results highlight a quasi systematic reduction of the RMSE after constraint (Figure 4), which makes us confident that our KCC method does not lead to spurious corrections. Even greater improvements of the posterior distributions are expected when constraining ASR and OLR projections instead of the EEI (Figure S9 in Supporting Information S1). This finding and other complementary results will be further discussed in the next section.

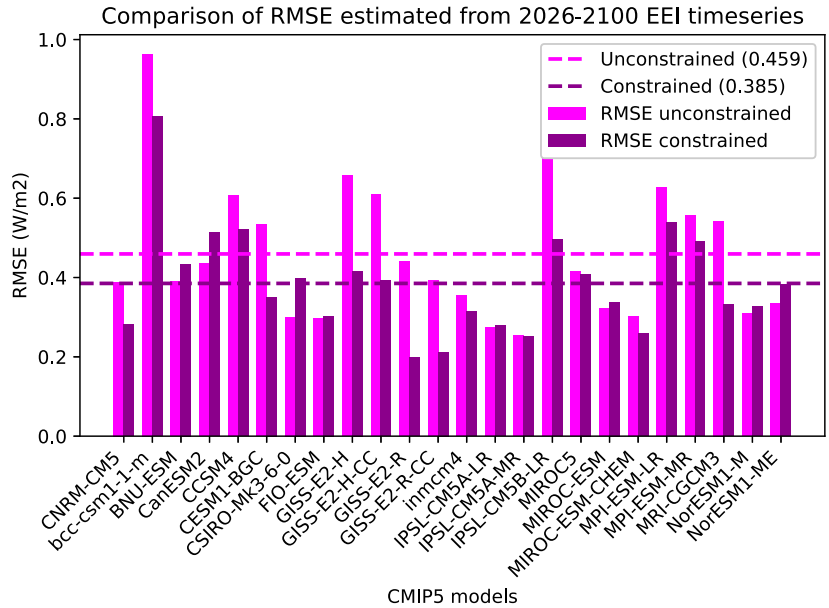

Figure 4. Summary of KCC performance to constrain EEI projections based on CMIP5 pseudo-observations. For each CMIP5 model (on the *x*-axis), the RMSE (in W/m^2) of the constrained versus unconstrained CMIP6 ensemble-mean forced response of the EEI is evaluated againt a raw and single realization of the selected CMIP5 model. The evaluation is made over the future 2026–2100 period, while the pseudo-obervational constraints are based on the past 1850–2025 and 1985–2023 periods for GSAT and EEI, respectively. The horizontal dashed lines denote the mean RMSE averaged across all CMIP5 pseudo-observations.

3. Discussion

Over recent years, the world has witnessed record GSAT, extreme North Atlantic SST and unprecedented extreme events at the regional scale. Detecting an acceleration of the Earth heating rate has however remained elusive in a context of high internal climate variability (e.g., Beaulieu et al., 2024; Jenkins et al., 2022; Raghuraman et al., 2023). The forced versus unforced origin of recent GSAT records has become a major debate in the climate change literature (e.g., Cheng et al., 2025; Samset et al., 2024), which has triggered a renewed interest in global EEI estimates (WMO, 2026).

In the present study, a global reconstruction of TOA radiative fluxes was used to constrain the EEI projections from a large subset of CMIP6 models. In line with the underestimation of the observed EEI trend, our results showed that the projected timing of the EEI trend reversal is biased in a majority of CMIP6 models. The application of KCC to the SSP1-2.6 low emission scenario led us to postpone the EEI stabilization by 3 years when considering the ensemble mean estimate (Figure 3). This adjusted timing is probably conservative given the difficulties that many countries are currently facing in achieving their GHG emissions targets. These results have potential implications for the remaining carbon budget and for the committed response of the slow components of the climate system.

Our method however relies on a number of hypotheses that must be here emphasized. It assumes a model-truth exchangeability (Ribes et al., 2021), meaning that the reality lies somewhere within the prior model distribution. While this may seem reasonable given the large sample of CMIP6 models, it is however challenged by the much higher rate of EEI increase in the DEEP-C reconstruction compared to CMIP6 historical simulations. Although internal variability is fully accounted for in the KCC method, the DEEP-C reconstruction (1985–2023) may be too short to isolate the forced response and does not provide any estimate of measurement uncertainties. This limitation has been circumvented by doubling the observed interannual variability and thus assuming a similar contribution of measurement uncertainty and interannual variability to the total uncertainty (cf. SI). Yet, this approximation may still be conservative and further monitoring the EEI will be crucial for confirming our results.

In the mean time, it is possible to repeat the KCC application by reducing rather than expanding the observed EEI record. Focusing on the CERES 2001–2023 instrumental record (Figure S10 in Supporting Information S1) does

not change our key conclusions. HadCRUT5 versus CERES observations lead to opposite changes in the mean forced EEI response, but their combination again indicates a later decline with a 25% reduction in the 5%–95% confidence interval. In line with the method evaluation (Figure S9 in Supporting Information S1), the parallel application of KCC to the ASR and OLR projections leads to a much stronger narrowing of CMIP6 modeling uncertainties (Figures S10d–S10i in Supporting Information S1), but still with an opposite influence of the individual observational constraints on the ensemble mean forced response.

These results suggest two possible directions for better constraining the EEI projections. The first one is the design of a multivariate KCC method where the ASR-OLR vector could be used instead of the EEI timeseries in order to constrain the EEI projections (see also Myhre et al., 2025). A second possibility would be to go beyond global mean metrics by exploring the patterns of both recent and future EEI changes. For instance, a Maximum Covariance Analysis (Bretherton et al., 1992) can be used to relate the patterns of recent trends in EEI or SAT versus future changes in EEI across our large set of CMIP6 models. In the first case (Figure S11 in Supporting Information S1), the leading singular vectors show highly correlated expansion coefficients ($R = 0.95$) but contrasted patterns over the Atlantic and Indian oceans. In the second case (Figure S12 in Supporting Information S1), the MCA results indicate a stronger Arctic amplification over recent decades is associated with a stronger heat uptake in the high latitudes (related to an earlier retreat of sea ice) and stronger positive EEI anomalies in the eastern and central tropical Pacific.

The later feature can be explained by a stronger zonal asymmetry in the future tropical Pacific warming (Figure S13 in Supporting Information S1). It is not found in the homogeneous vector, such suggesting a time-dependence of surface warming patterns. This finding is consistent with the study by Armour et al. (2024): discrepancies in the simulation of the observed warming pattern may result in a bias in the relationship between recent global warming and climate sensitivity (Figure S13d in Supporting Information S1).

Similar concerns may challenge the use of global mean EEI observations to constrain future global mean EEI projections. Despite this potential caveat, we are relatively confident that the stabilization of the Earth heating rate is very unlikely to occur before the early 2040s, in line with the lower bound of our 5%–95% confidence interval under the SSP1-2.6 low-emission scenario. This confidence relies on three pillars: the use of both GSAT and EEI observations, the overall performance of our KCC method when evaluated against independent pseudo-observations, and the lack of sensitivity to the choice of the prior (CMIP5 instead of CMIP6) or to the only use of the post-2000 CERES record.

Finally, our results are also consistent with previous related studies which have assessed the recent increase in EEI primarily as a forced response (Li et al., 2024; Raghuraman et al., 2021, 2023; Samset et al., 2025). The application of another Bayesian method has led to the same conclusion that this forced response is underestimated by most CMIP6 models (Li et al., 2024). This underestimation may however not be persistent if the observed trend is explained by improved air quality over East Asia (Samset et al., 2025) rather than by a lack of sensitivity to the GHG radiative forcing. Such a partitioning is still debated (Mauritsen et al., 2025; Minière et al., 2025) and deserves further investigation to better understand the apparent model failure to capture the recent increase in the observed Earth heating rate.

Conflict of Interest

The authors declare no conflicts of interest relevant to this study.

Availability Statement

All the data used in this study are publicly available online, including the HadCRUT5 data set of monthly mean surface temperature (Morice et al., 2020), the DEEP-C reconstruction of radiative fluxes (Liu & Allan, 2018) and the CMIP6 archive (Eyring et al., 2016). The KCC package (Qasmi & Ribes, 2022) is also available under a GNU General Public License. Other codes for data curation and plot drawings are basic Python applications but can be also easily reproduced with your own favorite graphic tools. All data needed to evaluate the conclusions in the paper are present in the paper and/or the Supporting Information S1.

Acknowledgments
The authors are grateful to all global modelling centers which have contributed to CMIP6, as well as to the people in charge of the ESGF archive (https://esgf-node.llnl.gov/projects/cmip6/) and of the ESPRI platform (https://mesocentre.ipsl.fr/plate-forme-physique/). Thanks are also due to two anonymous reviewers for their useful comments. The study received no funding.

References

Allan, R. P., & Merchant, C. J. (2025). Reconciling Earth's growing energy imbalance with ocean warming. *Environmental Research Letters*, *20*(4), 044002. https://doi.org/10.1088/1748-9326/adb448

Armour, K. C., Proistosescu, C., Dong, Y., Hahn, L. C., Blanchard-Wrigglesworth, E., Pauling, A. G., et al. (2024). Sea-surface temperature pattern effects have slowed global warming and biased warming-based constraints on climate sensitivity. *Proceedings of the National Academy of Sciences of the United States of America*, *121*(12), e2312093121. https://doi.org/10.1073/pnas.2312093121

Beaulieu, C., Gallagher, C., Killick, R., Lund, R., & Shi, X. (2024). A recent surge in global warming is not detectable yet. *Communications Earth & Environment*, *5*(1), 576. https://doi.org/10.1038/s43247-024-01711-1

Bretherton, C. S., Smith, C., & Wallace, J. M. (1992). An intercomparison of methods for finding coupled patterns in climate data. *Journal of Climate*, *5*(6), 541–560. https://doi.org/10.1175/1520-0442(1992)005<0541:aiomff>2.0.co;2

Cheng, L., Abraham, J., Trenberth, K. E., Reagan, J., Zhang, H. M., Storto, A., et al. (2025). Record high temperatures in the ocean in 2024. *Advances in Atmospheric Sciences*, *42*(6), 1092–1109. https://doi.org/10.1007/s00376-025-4541-3

Douville, H. (2023). Robust and perfectible constraints on human-induced Arctic climate change. *Communications Earth & Environment*, *4*(1), 283. https://doi.org/10.1038/s43247-023-00949-5

Douville, H., & Plazzotta, M. (2017). Midlatitude summer drying: An underestimated threat in CMIP5 models? *Geophysical Research Letters*, *44*, 9967–9975. https://doi.org/10.1002/2017GL075353

Douville, H., Qasmi, S., Ribes, A., & Bock, O. (2022). Global warming at near-constant tropospheric relative humidity is supported by observations. *Communications Earth & Environment*, *3*(1), 237. https://doi.org/10.1038/s43247-022-00561-z

Douville, H., & Willett, K. (2023). A drier than expected future, supported by near-surface relative humidity observations. *Science Advances*, *9*(30), eade6253. https://doi.org/10.1126/sciadv.ade6253

Eyring, V., Bony, S., Meehl, G. A., Senior, C. A., Stevens, B., Stouffer, R. J., & Taylor, K. E. (2016). Overview of the coupled model intercomparison project phase 6 (CMIP6) experimental design and organization [Dataset]. *Geoscientific Model Development*, *9*(5), 1937–1958. https://doi.org/10.5194/gmd-9-1937-2016

Ferguglia, O., von Hardenberg, J., & Palazzi, E. (2023). Robustness of precipitation Emergent constraints in CMIP6 models. *Climate Dynamics*, *61*(3–4), 1439–1450. https://doi.org/10.1007/s00382-022-06634-1

Forster, P. M., Smith, C., Walsh, T., Lamb, W. F., Lamboll, R., Cassou, C., et al. (2025). Indicators of global climate change 2024: Annual update of key indicators of the state of the climate system and human influence. *Earth System Science Data*, *17*(6), 2641–2680. https://doi.org/10.5194/essd-17-2641-2025

Forster, P. T., Storelvmo, T., Armour, K., Collins, W., Dufresne, J.-L., Frame, D., et al. (2021). The Earth's energy budget, climate feedbacks and climate sensitivity. In V. Masson-Delmotte, P. Zhai, A. Pirani, et al. (Eds.), *Climate change 2021: The physical science basis. Contribution of working Group I to the sixth assessment report of the intergovernmental panel on climate change*. Cambridge University Press. https://doi.org/10.1017/9781009157896

Goessling, H. F., Rackow, T., & Jung, T. (2024). Recent global temperature surge intensified by record-low planetary albedo. *Science*, *287*, eadq7280.

Hersbach, H., Bell, B., Berrisford, P., Biavati, G., Horányi, A., Muñoz Sabater, J., et al. (2020). The ERA5 global reanalysis. *Quarterly Journal Royal Meteorological Society*, *146*(730), 1999–2049. https://doi.org/10.1002/qj.3803

Hodnebrog, O., Myhre, G., Jouan, C., Andrews, T., Forster, P. M., Jia, H., et al. (2024). Recent reductions in aerosol emissions have increased Earth's energy imbalance. *Communications Earth & Environment*, *5*(1), 166. https://doi.org/10.1038/s43247-024-01324-8

Jenkins, S., Povey, A., Gettelman, A., Grainger, R., Tier, P. S., & Allen, M. (2022). Is anthropogenic global warming accelerating? *Journal of Climate*, *35*(24), 7873–7890. https://doi.org/10.1175/jcli-d-22-0081.1

Li, C., Liu, J., Du, F., Zwiers, F. W., & Feng, G. (2025). Increasing certainty in projected local extreme precipitation change. *Nature Communications*, *16*(1), 850. https://doi.org/10.1038/s41467-025-56235-9

Li, C., Zwiers, F. W., Zhang, X., Fischer, E. M., Du, F., Liu, J., et al. (2025). Constraining the entire Earth system projections for more reliable climate change adaptation planning. *Science Advances*, *11*(9), eadr5346. https://doi.org/10.1126/sciadv.adr5346

Li, X., Li, Q., Wild, M., & Jones, P. (2024). An intensification of surface Earth's energy imbalance since the late 20th century. *Communications Earth & Environment*, *5*(1), 644. https://doi.org/10.1038/s43247-024-01802-z

Liu, C., & Allan, R. P. (2018). Reconstructions of the radiation fluxes at the top of atmosphere and net surface energy flux: DEEP-C version 5.0 [Dataset]. The University of Reading. Retrieved from https://researchdata.reading.ac.uk/347/

Liu, C., Allan, R. P., Mayer, M., Hyder, P., Desbruyères, D., Cheng, L., et al. (2020). Variability in the global energy budget and transports 1985–2017. *Climate Dynamics*, *55*(11–12), 3381–3396. https://doi.org/10.1007/s00382-020-05451-8

Loeb, N. G., Doelling, D. R., Wang, H., Su, W., Nguyen, V., Corbett, J. G., et al. (2018). Clouds and the Earth's radiant energy system (CERES) energy balanced and filled (EBAF) top-of-atmosphere (TOA) edition-4.0 data product [Dataset]. *Journal of Climate*, *31*(2), 895–918. https://doi.org/10.1175/jcli-d-17-0208.1

Loeb, N. G., Ham, S. H., Allan, R. P., Thorsen, T. J., Meyssignac, B., Kato, S., et al. (2024). Observational assessment of changes in Earth's energy imbalance since 2000. *Surveys in Geophysics*, *45*(6), 1757–1783. https://doi.org/10.1007/s10712-024-09838-8

Mauritsen, T., Tsushima, Y., Meyssignac, B., Loeb, N. G., Hakuba, M., Pilewskie, P., et al. (2025). Earth's energy imbalance more than doubled in recent decades. *AGU Advances*, *6*(3), e2024AV001636. https://doi.org/10.1029/2024AV001636

Merchant, C. J., Allan, R. P., & Embury, V. (2025). Quantifying the acceleration of multidecadal global sea surface warming driven by Earth's energy imbalance. *Environmental Research Letters*, *20*(2), 024037. https://doi.org/10.1088/1748-9326/adaa8a

Minière, A., von Schuckmann, K., Sallée, J.-B., & Vogt, L. (2025). Robust acceleration of Earth system heating observed over the past six decades. *Scientific Reports*, *13*(1), 22975. https://doi.org/10.1038/s41598-023-49353-1

Morice, C. P., Kennedy, J. J., Rayner, N. A., Winn, J. P., Hogan, E., Killick, R. E., et al. (2020). An updated assessment of near-surface temperature change from 1850: The HADCRUT5 data set [Dataset]. *Journal of Geophysical Research: Atmospheres*, *126*(3). https://doi.org/10.1029/2019jd032361

Myhre, G., Hodnebrog, O., Loeb, N., & Forster, P. M. (2025). Observed trend in Earth energy imbalance may provide a constraint for low climate sensitivity models. *Science*, *388*(6752), 1210–1213. https://doi.org/10.1126/science.adt0647

Olonscheck, D., & Rugenstein, M. (2024). Coupled climate models systematically underestimate radiation response to surface warming. *Geophysical Research Letters*, *51*(6), e2023GL106909. https://doi.org/10.1029/2023GL106909

Qasmi, S., & Ribes, A. (2022). Reducing uncertainty in local temperature projections [Software]. *Science Advances Zenodo*, *8*, 41. https://doi.org/10.5281/zenodo.5233947

Raghuraman, S. P., Paynter, D., Menzel, R., & Ramaswamy, V. (2023). Forcing, cloud feedbacks, cloud masking, and internal variability in the cloud radiative effect satellite record. *Journal of Climate*, *36*(12), 4151–4167. https://doi.org/10.1175/jcli-d-22-0555.1

Raghuraman, S. P., Paynter, D., & Ramaswamy, V. (2021). Anthropogenic forcing and response yield observed positive trend in Earth's energy imbalance. *Nature Communications*, *12*(1), 4577. https://doi.org/10.1038/s41467-021-24544-4

Ribes, A., Qasmi, S., & Gillett, N. (2021). Making climate projections conditional on historical observations. *Science Advances*, *7*(4), eabc0671. https://doi.org/10.1126/sciadv.abc0671

Samset, B. H., Lund, M. T., Fuglestvedt, J. S., & Wilcox (2024). 2023 temperatures reflect steady global warming and internal sea surface temperature variability. *Communications Earth & Environment*, *5*(1), 460. https://doi.org/10.1038/s43247-024-01637-8

Samset, B. H., Wilcox, L. J., Allen, R. J., Stjern, C. W., Lund, M. T., Ahmadi, S., et al. (2025). East Asian aerosol cleanup has likely contributed to the recent acceleration in global warming. *Communications Earth & Environment*, *6*(1), 543. https://doi.org/10.1038/s43247-025-02527-3

Sanderson, B. M., Pendergrass, A. G., Koven, C. D., Brient, F., Booth, B. B. B., Fisher, R. A., & Knutti, R. (2021). The potential for structural errors in emergent constraints. *Earth System Dynamics*, *12*, 899–918.

Schlund, M., Lauer, A., Gentine, P., Sherwood, S. C., & Eyring, V. (2020). Emergent constraints on equilibrium climate sensitivity in CMIP5: Do they hold for CMIP6? *Earth System Dynamics*, *11*(4), 1233–1258. https://doi.org/10.5194/esd-11-1233-2020

Skeie, R. B., Aldrin, M., Berntsen, T. K., Holden, M., Huseby, R. B., Myhre, G., & Storelvmo, T. (2024). The aerosol pathway is crucial for observationally constraining climate sensitivity and anthropogenic forcing. *Earth System Dynamics*, *15*(6), 1435–1458. https://doi.org/10.5194/esd-15-1435-2024

Smith, G. L., Priestley, K., Loeb, N., Wielicki, B., Charlock, T., Minnis, P., et al. (2011). Clouds and Earth radiant energy system (CERES), a review: Past, present and future. *Advances in Space Research*, *48*(2), 254–263. https://doi.org/10.1016/j.asr.2011.03.009

Storto, A., & Yang, C. (2024). Acceleration of the ocean warming from 1961 to 2022 unveiled by large-ensemble reanalyses. *Nature Communications*, *15*(1), 545. https://doi.org/10.1038/s41467-024-44749-7

Tokarska, K. B., Stolpe, M. B., Sippel, S., Fischer, E. M., Smith, C. J., Lehner, F., & Knutti, R. (2020). Past warming trend constrains future warming in CMIP6 models. *Science Advances*, *6*(12), eaaz9549. https://doi.org/10.1126/sciadv.aaz9549

Von Schuckmann, K., Minière, A., Gues, F., Cuesta-Valero, F. J., Kirchengast, G., Adusumilli, S., et al. (2023). Heat stored in the Earth system 1960–2020: Where does the energy go? *Earth System Science Data*, *15*(4), 1675–1709. https://doi.org/10.5194/essd-15-1675-2023

WMO. (2026). *State of the global climate 2025. WMO-No. 1391*. World Meteorological Organization, 2026. https://doi.org/10.59327/WMO/S/CRI/SOC1